

# Mechanism and uses of a membrane peptide that targets tumors and other acidic tissues *in vivo*

Oleg A. Andreev\*<sup>†</sup>, Allison D. Dupuy<sup>†</sup>, Michael Segala\*, Srikanth Sandugu\*, David A. Serra<sup>‡</sup>, Clinton O. Chichester<sup>§</sup>, Donald M. Engelman<sup>†¶</sup>, and Yana K. Reshetnyak\*<sup>†¶</sup>

\*Physics Department, University of Rhode Island, 2 Lippitt Road, Kingston, RI 02881; <sup>†</sup>Department of Molecular Biophysics and Biochemistry, Yale University, P.O. Box 208114, New Haven, CT 06520; <sup>‡</sup>Research Office, University of Rhode Island, 70 Lower College Road, Kingston, RI 02881; and <sup>§</sup>Department of Biomedical and Pharmaceutical Sciences, University of Rhode Island, Fogarty Hall, 41 Lower College Road, Kingston, RI 02881

Contributed by Donald M. Engelman, March 17, 2007 (sent for review December 19, 2006)

The pH-selective insertion and folding of a membrane peptide, pHLIP [pH (low) insertion peptide], can be used to target acidic tissue *in vivo*, including acidic foci in tumors, kidneys, and inflammatory sites. In a mouse breast adenocarcinoma model, fluorescently labeled pHLIP finds solid acidic tumors with high accuracy and accumulates in them even at a very early stage of tumor development. The fluorescence signal is stable for >4 days and is approximately five times higher in tumors than in healthy counterpart tissue. In a rat antigen-induced arthritis model, pHLIP preferentially accumulates in inflammatory foci. pHLIP also maps the renal cortical interstitium; however, kidney accumulation can be reduced significantly by providing mice with bicarbonate-containing drinking water. The peptide has three states: soluble in water, bound to the surface of a membrane, and inserted across the membrane as an  $\alpha$ -helix. At physiological pH, the equilibrium is toward water, which explains its low affinity for cells in healthy tissue; at acidic pH, titration of Asp residues shifts the equilibrium toward membrane insertion and tissue accumulation. The replacement of two key Asp residues located in the transmembrane part of pHLIP by Lys or Asn led to the loss of pH-sensitive insertion into membranes of liposomes, red blood cells, and cancer cells *in vivo*, as well as to the loss of specific accumulation in tumors. pHLIP nanotechnology introduces a new method of detecting, targeting, and possibly treating acidic diseased tissue by using the selective insertion and folding of membrane peptides.

cancer targeting | imaging | peptide insertion

Many pathological conditions such as cancer, ischemic stroke, inflammation, atherosclerotic plaques, and others are associated with increased metabolic activity and hypoxia resulting in an elevated extracellular acidity (1–6). Hypoxia and acidity have emerged as important factors in tumor biology and responses to cancer treatment. Imaging of hypoxic and acidic regions could provide new information about disease localization and progression and might enhance diagnosis and therapy. Here we describe the use of a peptide, pHLIP [pH (low) insertion peptide], to selectively accumulate in and label acidic tissues. We previously reported that the pHLIP bionanosyringe, a 36-aa peptide derived from the bacteriorhodopsin C helix, has three states: soluble in water, bound to the surface of a membrane, and inserted across the membrane as an  $\alpha$ -helix. At physiological pH the water-soluble form is favored, whereas at acidic pH the transmembrane  $\alpha$ -helix predominates (Fig. 1*a*) (7). We show that at low pH, pHLIP can translocate cell-impermeable cargo molecules that are disulfide-linked to the C terminus across a cell membrane, where they are released in the cytoplasm by reduction of the disulfide bond (8, 9). Among the successfully translocated molecules are organic dyes, phalloidin (a polar, cyclic peptide), and a 12-mer peptide nucleic acid.

## Results

We applied the technique of near-infrared (NIR) fluorescence imaging to follow the ability of fluorescently labeled pHLIP and its variants to accumulate in tissue with low extracellular pH by using

mouse cancer and rat inflammatory arthritis models. Light with wavelengths in the NIR range (700–900 nm) can propagate through tissue for distances on the order of multiple centimeters because of low tissue and water absorption in that range. NIR fluorescence imaging offers unique advantages for the imaging of pathophysiological states and is well suited to studies of small animals, tissues, organs, and whole bodies (10–12). NIR fluorescent dyes were conjugated with Cys or Lys residues placed on the pHLIP N terminus, which remains outside of the cell when the peptide inserts across the lipid bilayer (8). Two different fluorescent probes (Cy5.5 or Alexa750) were used in the study to exclude any possibility of specific accumulation of a particular dye in the tissue. Alexa750 absorbs and emits at longer wavelengths than does Cy5.5 and has different physicochemical properties.

Three imaging systems with different imaging capabilities were used in the study: a homemade imager, an Odyssey IR scanner (Li-Cor, Lincoln, NE), and a Kodak FX *In Vivo* Image Station (Eastman Kodak, New Haven, CT). The homemade imager consists of a light source (150-W xenon lamp) with double fiber-optic gooseneck, NIR-CCD camera, and filters, allowing us to perform surface imaging. However, the IR scanner with a variable focal distance (up to 4 mm) and extremely sensitive recording system consisting of avalanche diodes allowed us to collect light from the interior of the body with great sensitivity. An FX Kodak *in vivo* image station was used to obtain both fluorescence and x-ray images.

pHLIP-NIR dye constructs injected into mice bearing breast adenocarcinoma show significant accumulation in tumors (Fig. 1*b*), even very small ones (Fig. 1*c*). Injection of fluorescent pHLIP and tumor imaging were performed 4–21 days after cancer-cell implantation to mimic various stages of tumor development from early to advanced. pHLIP was given as a single i.p. injection into the left side of mice with breast adenocarcinoma in their right flanks. pHLIP-fluorescent dyes were redistributed and concentrated in tumors within 20 h after injection (Fig. 1*d*). pHLIP was able to mark tumors of various sizes (Fig. 1*e–h*), even those that were visually undetectable. A small fluorescent spot is clearly observed in the location of the tumor-cell injection (Fig. 1*e*), and a visible tumor appeared at the location of the fluorescence after several days.

As another model of low pH, we used a rat inflammatory arthritis model. Arthritis was induced in the right knee joints by using methylated BSA and Freund's complete adjuvant (13). The arthritis

Author contributions: O.A.A., A.D.D., C.O.C., D.M.E., and Y.K.R. designed research; O.A.A., A.D.D., M.S., S.S., D.A.S., C.O.C., and Y.K.R. performed research; C.O.C. and Y.K.R. contributed new reagents/analytic tools; O.A.A., A.D.D., D.A.S., C.O.C., D.M.E., and Y.K.R. analyzed data; and O.A.A., A.D.D., D.M.E., and Y.K.R. wrote the paper.

The authors declare no conflict of interest.

Freely available online through the PNAS open access option.

Abbreviations: pHLIP, pH (low) insertion peptide; NIR, near infrared; RBC, red blood cell; CI, contrast index.

<sup>¶</sup>To whom correspondence may be addressed. E-mail: donald.engelman@yale.edu or reshetnyak@mail.uri.edu.

© 2007 by The National Academy of Sciences of the USA

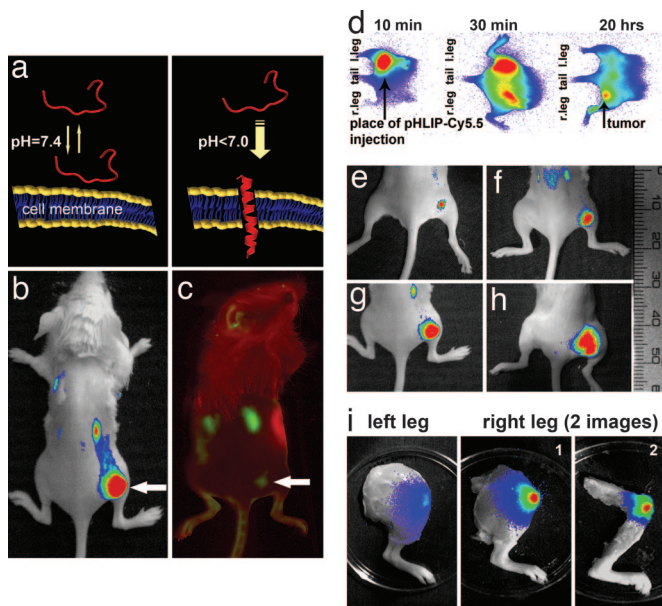


**Fig. 1.** Imaging tumors and inflammation. (a) The mechanism of pHLIP interaction with lipid bilayers. The peptide has three states: soluble in water, bound to the surface of a membrane (at normal pH 7.4), and inserted across the membrane as an  $\alpha$ -helix (at low pH). (b) Overlay of pHLIP-Cy5.5 fluorescence and light images of mice bearing a tumor (7 mm in diameter, 12 d after  $10^6$  cell implant) in the right flank obtained on the homemade imager (i.p. injection of 500  $\mu$ g/kg of pHLIP-Cy5.5 1 d before imaging). (c) pHLIP-Alexa750 fluorescent image (excitation 750 nm, emission 800 nm, artificial green color) of mice bearing a tumor (2 mm in diameter 6 d after  $10^6$  cell implant) in the right flank obtained on the IR scanner with focal distance set at 3 mm, which allows for the collection of light from the interior of the body (i.p. injection of 300  $\mu$ g/kg of pHLIP-Alexa750 1 d before imaging). Reflectance is denoted in red (excitation 680 nm). (d) pHLIP-Cy5.5 given as a single i.p. injection (200  $\mu$ g/kg) into the left side of mice initially diffused into the left flank, but 20 h later it accumulated in a tumor on the right flank. The fluorescent image of the back part of each mouse is presented. Blue color represents the background fluorescent signal, and the red color represents a high intensity of the fluorescence signal. (e–h) Overlay of pHLIP-Cy5.5 (500  $\mu$ g/kg) fluorescence and light images of back part of mice bearing tumors of different sizes in right flanks: (e) undetectable by eye at time of imaging 5 d after  $10^5$  cell implant, (f)  $3 \times 4$  mm (8 d after  $10^6$  cell implant), (g)  $5 \times 6$  mm (12 d after  $10^6$  cell implant), (h)  $8 \times 9$  mm (18 d after  $10^6$  cell implant). (i) Accumulation of pHLIP-Cy5.5 (2 days after i.p. injection, 30  $\mu$ g/kg) in inflammation sites is shown by overlay of pHLIP fluorescence and photo images of rat right (arthritis) and left (control) legs. The arthritis was induced in the right leg by injection of methylated BSA and Freund's complete adjuvant (the left knee of the rat received a sham injection of saline and was used as a control). A substantial fluorescence signal (4–5 times higher than in the left knee joint) was detected in the right knee (1), especially in the knee joint (2) (red color represents high fluorescence intensity).

in this model is induced by inflammatory activity and associated with the acidification of soft tissue and synovial fluid (14, 15). First, whole-body imaging was performed (data not shown). The animals then were killed, and their right and left legs were imaged separately. Then, skin and muscle were removed from the legs followed by fluorescence imaging of the knee joints. pHLIP-Cy5.5 targets sites of inflammation in the right leg with no accumulation in the left (control) leg (Fig. 1i). The right leg, and especially the knee joints, were analyzed. A substantial fluorescence signal (4–5 times higher than in the left knee joints) was detected in the right knee joints (Fig. 1i, 1 and 2). The results of whole-body fluorescence imaging indicate that pHLIP is stable enough to reach and accumulate in the acidic environment associated with various pathological processes.

To check the specificity of pHLIP accumulation in tumors and test the molecular mechanism of pHLIP insertion, we designed two peptide variants (N-pHLIP and K-pHLIP):

- pHLIP: ACEQNPIYWARYADWLF~~T~~TP~~L~~LLL~~L~~DLALLVD-ADEGTG
- N-pHLIP: ACEQNPIYWARYANWLF~~T~~TP~~L~~NLL~~L~~NLALLV-DADEGTG
- K-pHLIP: ACEQNPIYWARYAKWLF~~T~~TP~~L~~KLL~~L~~KLALLV-DADEGTG.

In N-pHLIP and K-pHLIP, Asn and Lys replaced Asp residues, one of which is protonated at low pH and drives pHLIP insertion (7–9). The interactions of pHLIP and its variants with lipid bilayers were studied by using liposomes, human red blood cells (RBCs), and cancer cells in a mouse model. Fluorescence of two Trp residues located in the transmembrane part of the peptides is sensitive to the insertion process (7) and can be used to monitor it. Insertion is accompanied by the translocation of Trp fluorophores from the hydrophilic aqueous solution into the hydrophobic environment of a lipid bilayer, resulting in enhancement of emission and a shift of the spectrum to short wavelengths (16) (Fig. 2a). Formation of  $\alpha$ -helical secondary structure is monitored by using changes in the circular dichroism (CD) signal (Fig. 2b). It was previously demonstrated by polarized FTIR that the orientation of pHLIP is perpendicular to the lipid bilayer at low pH (7), which is part of the evidence for a transmembrane  $\alpha$ -helix.

Unlike pHLIP, K-pHLIP does not show secondary structure changes between normal and low pH in the presence of liposomes. However, K-pHLIP is more aggregated in solution (the position of maximum of the fluorescence spectrum is shifted to short wavelengths) than pHLIP and exhibits partial  $\alpha$ -helical structure at normal pH in the absence of liposomes. In contrast to the other peptides, N-pHLIP forms  $\alpha$ -helical structure in the presence of liposomes over a wide pH range (4.0–8.0). Trp fluorescence and CD spectra indicate that K-pHLIP remains outside of the membrane at all pH levels studied, whereas N-pHLIP is mostly in the membrane.

To further study the interaction of the peptides with a membrane, we performed experiments on human RBCs. As an important experimental measure, it was essential to test whether pHLIP damages RBCs when it is injected into the bloodstream. The lytic response of pHLIP was measured spectrophotometrically by the amount of released hemoglobin from human RBCs. Human RBCs incubated in isotonic buffers at pH 6.0 and 7.4 at room temperature served as negative controls. As a positive control of 100% lysis, human RBCs were opened by incubation with 10% Triton X-100 for 1 h at room temperature. The results indicate that pHLIP does not lyse RBCs at concentrations up to 10  $\mu$ M.

Next, we characterized the effect of pHLIP on RBC membrane morphology. The RBC has a very flexible membrane, consisting of a plasma membrane attached to an intricate membrane skeleton. It is well known that various agents interacting with RBCs can modify the biconcave discoid shape (discocyte; Fig. 2c) of these cells (17, 18). Selective insertion of molecules into the outer leaflet of RBCs leads to an increase in the relaxed area difference between the two leaflets of the plasma membrane bilayer, resulting in the formation of convex structures on the cell surface (e.g., echinocytic spicules; Fig. 2c) (19–21). The interaction of pHLIP with RBCs at normal pH (7.4; when the peptide attaches to the cell surface without the formation of any elements of secondary structure) results in the appearance of spicules on the surface of 67% of the cells (Fig. 2d and Table 1), showing extra area occupied by pHLIP on the outer leaflet of the lipid bilayer. However, a significantly reduced number of spikes were seen (87% of cells have a smooth, biconcave discoid shape) when pHLIP was inserted into the membrane at low pH (6.0), consistent with insertion across both halves of the bilayer. K-pHLIP induces formation of echinocytes at both normal and low pH (57% and 55% of cells, respectively), suggesting that the peptide weakly binds to the membrane surface at both pH levels. N-pHLIP does not induce significant shape changes in RBCs at normal or low pH (74% and 83% of the cells, respectively, are discocytes).

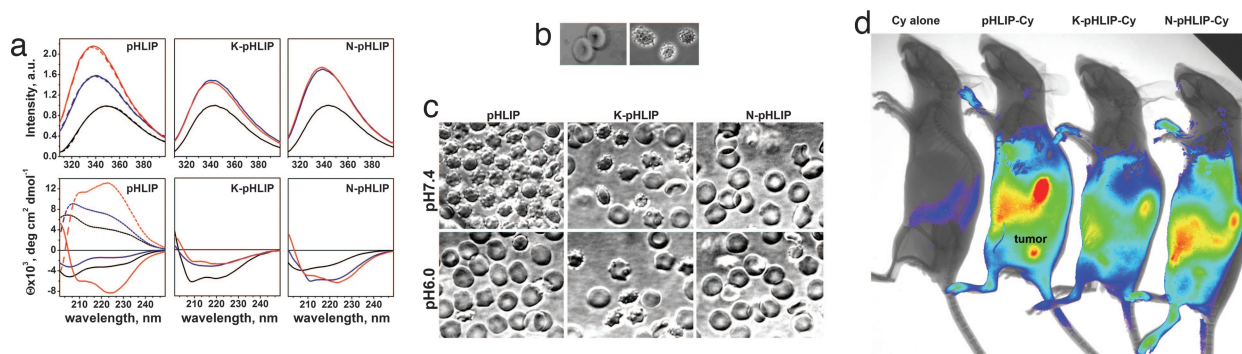


**Fig. 2.** Interaction of pHLIP and its variants with membranes of liposomes, human RBCs, and cancer cells *in vivo*. Trp fluorescence (a) and CD (b) spectra of pHLIP [consisting of L-amino acids (solid lines) and D-amino acids (dotted lines)], K-pHLIP, and N-pHLIP were recorded to monitor the process of their interaction with 1-palmitoyl-2-oleoyl-*sn*-glycero-3-phosphocholine liposomes at normal and low pH. The fluorescence excitation wavelength was 295 nm for the excitation of Trp fluorophores. The concentrations of peptides and lipids were 5 and 600  $\mu\text{M}$ , respectively. Black signifies fluorescence and CD spectra of pHLIP at pH 8.0 in the absence of liposomes; blue, after 30 min of incubation with liposomes at pH 8.0; red, after incubation with liposomes at pH 4.5. (c) Binding of various agents selectively to the outer leaflet of RBCs can change the biconcave discoid shape of the cells (left image) into convex structures on the cell surface (right image), echinocytic spicules. (d) Phase-contrast images of 1% suspensions of human RBCs incubated for 15 min with 5  $\mu\text{M}$  pHLIP, K-pHLIP, and N-pHLIP at pH 7.4 and 6.0 are presented. RBCs without peptides had normal discoid shape at both pH 7.4 and 6.0 (images are not shown). Statistical data (percentage of cells having spicules) are shown in Table 1. To avoid induction of echinocytosis by proximity to a glass surface, glass slides were treated with 2% dimethyldichlorosilane in 1,1,1-trichloromethane for 10 min and rinsed with methanol, ethanol, and water and allowed to dry before use in experiments. Grace Bio-Labs (Bend, OR) CoverWell imaging chambers were used for observation of RBC/peptide suspensions instead of glass coverslips. The pictures were taken on an Olympus IX71 inverted-fluorescence microscope with an  $\times 100$  objective. (e) Overlay of NIR fluorescence and x-ray images obtained by using a Kodak In-Vivo FX image station on the next day after i.p. injection of 500  $\mu\text{g}/\text{kg}$  pHLIP-Cy5.5, K-pHLIP-Cy5.5, N-pHLIP-Cy5.5, or molar equivalent amount of Cy5.5 alone on mice bearing tumors in the right flank. The injection of peptide was performed when the tumor was not detectable by eye on the sixth day after cancer-cell implantation ( $5 \times 10^4$  cells); imaging was performed on the next day. Tumors became visible 2 weeks later. Replacement of two key Asp residues located in the transmembrane part of pHLIP by Lys or Asn leads to the loss of pH-sensitive insertion into membranes of liposomes, RBCs, and cancer cells *in vivo*, as well as to the loss of specific accumulation in tumors.

Fluorescence and CD data indicate that N-pHLIP interacts with lipid vesicles and forms  $\alpha$ -helical structure at both pHs. The RBC data support the idea that N-pHLIP inserts in lipid bilayers as a transmembrane  $\alpha$ -helix, whereas the positively charged Lys residues prevent insertion of K-pHLIP into the hydrophobic core of the lipid bilayer at both normal and low pH levels. The dramatic RBC shape changes induced by pHLIP at normal pH and their absence at low pH are in agreement with the mechanism seen in lipid vesicles.

The ability of pHLIP and its variants to find a tumor and accumulate in it at very early stages of tumor development was evaluated *in vivo*. To create slow-growing tumors,  $5 \times 10^4$  JC mouse breast adenocarcinoma cells were injected s.c. in the right flanks of mice. Tumors became visible in 16–18 days (1–3 mm in diameter). pHLIP was able to detect such slow-growing tumors on day 6. Fig. 2e shows NIR images of mice with early tumors 1 day after the i.p. injection of Cy5.5 alone, pHLIP-Cy5.5, K-pHLIP-Cy5.5, and N-pHLIP-Cy5.5. Two weeks later, tumors of similar size and shape in the right flanks became visible in all mice. The accumulation of dye alone or of the pHLIP variants in tumors was insignificant in comparison with pHLIP. It is interesting to note that the background signal from K-pHLIP was very weak, and the peptide was cleared rapidly from the mouse. The fluorescence signal from

N-pHLIP was significant at the injection site and its vicinity, and it remained there for a long time, consistent with its local insertion in membranes. The imaging data *in vivo* confirm the proposed molecular mechanism of pHLIP action and show the ability of pHLIP to target tumors at very early stages of their development.

We examined the level of pHLIP accumulation in tumors. Fig. 3a shows 3D NIR emission intensity presentations of images of a tumor ( $4 \times 5$  mm in size) site taken during the 8 days after pHLIP-Cy5.5 injection. The height ( $z$  axes) and intensity of red color indicate the strength of the NIR signal in the right flank of a mouse in which the tumor was implanted. The fluorescence signal was very strong and stable for 4 days, approximately five times higher in tumors in comparison with the healthy counterpart tissue [see values of the contrast index (CI) in Fig. 3c]. In previous studies, accumulation in a tumor was considered substantial if the CI values were in the range of 2.5–3.5 (for 100  $\mu\text{l}$  of 60  $\mu\text{M}$  of peptide-dye injection) (22). Our data show that pHLIP is stable enough to persist in tumors. Insertion in the cell membrane may protect the peptide from attack by proteases, allowing it to accumulate in tumor tissue in significant amounts.

Where else does pHLIP accumulate besides the tumor? We collected organs and tissues on the second day after injection of the pHLIP-NIR dye (Fig. 3b and d). Whole-body fluorescence images, as well as fluorescence of individual organs, indicate that pHLIP accumulates in tumors and the kidney, the latter being a major site in the catabolism of low-molecular-weight proteins and having acidic regions. Buffering the feed water to pH 8.2 results in an elevation of the renal tubular and cortical interstitial pH (23). Indeed, we observed a significant reduction ( $\approx 50\%$ ) of the fluorescent signal in the kidneys of mice fed with water at pH 8.2 (Fig. 3e), supporting the idea that low pH causes the observed imaging. pHLIP allowed us to map the acidic areas in the kidney.

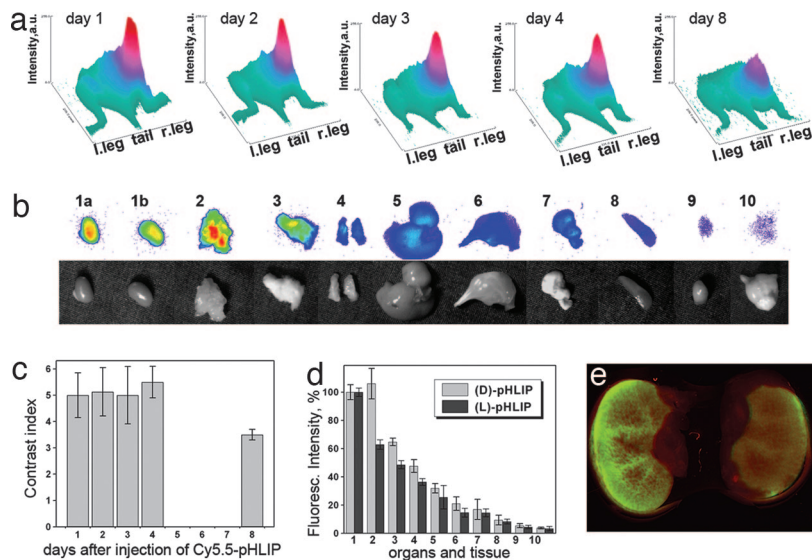
Experiments with pHLIP consisting of L-amino acids and D-amino acids gave similar results: accumulation in tumor, inflammatory foci, and kidney. The results confirm that the mechanism of peptide insertion is the formation of a transmembrane  $\alpha$ -helix, a process that does not depend on amino acid chirality. Interestingly,

**Table 1.** Human RBCs were used to probe the interaction of pHLIP and its variants with lipid bilayers at various pH levels

pH	RBCs,	RBCs + pHLIP,	RBCs + K-pHLIP,	RBCs + N-pHLIP,
	%	%	%	%
7.4	$14.3 \pm 5.8$	$67.3 \pm 12.6$	$57.3 \pm 8.9$	$25.8 \pm 4.1$
6.0	$16.2 \pm 6.2$	$12.6 \pm 4.0$	$55.5 \pm 7.3$	$17.1 \pm 5.9$

The percentage of RBCs having spicules on the surface was calculated from the phase-contrast images of 1% suspensions of human RBCs incubated for 15 min with 5  $\mu\text{M}$  pHLIP, K-pHLIP, and N-pHLIP at pH 7.4 and 6.0. A high percentage of spicule formation is interpreted as a visualization of the interaction of peptides with the outer leaflet of RBCs, which leads to an increase in the relaxed area difference between the two leaflets of the plasma membrane and consequent distortion of the biconcave discoid shape of the cells.

**Fig. 3.** CI and distribution of pHLIP in organs. (a) The 3D presentation of NIR fluorescence images of mice bearing a tumor (4 × 5 mm size) 8 days after i.p. injection of 500 μg/kg of pHLIP-Cy5.5, which was done on the seventh day of tumor growth. The height (z axes) and intensity of red color indicate the strength of the NIR signal in the right flank of a mouse where the tumor was implanted. (b) NIR fluorescence and light images of kidneys (1 a and b), tumor (2), skin (3), stomach cleaned and separated into 2 parts (4), liver (5), muscle (6), lung (7), spleen (8), heart (9), and brain (10) collected from a mouse bearing a tumor on the next day after injection of 500 μg/kg of pHLIP-Cy5.5 consisting of L-amino acids or D-amino acids. (c) The CI, which indicates the relative strength of the fluorescence signal in tumors, was calculated as a ratio:  $CI = [(F_{\text{tumor}} - F_{\text{auto}})/(F_{\text{norm}} - F_{\text{auto}})]$ .  $F_{\text{tumor}}$  and  $F_{\text{norm}}$  are the mean fluorescence intensities of tumor and normal contralateral regions of the same area, respectively, and  $F_{\text{auto}}$  is the autofluorescence from the corresponding region measured before injection. The fluorescence signal from the tumor was approximately five times stronger in comparison with the contralateral region. The CI was calculated for >20 animals. (d) The fluorescence signals were measured from organs collected the next day after i.p. injection of 500 μg/kg of pHLIP-Cy5.5 consisting of L-amino acids and D-amino acids. The signals were normalized to the intensity of kidney fluorescence. (e) The NIR fluorescence of kidney 2 days after i.p. injection of 500 μg/kg of pHLIP-Alexa750 into mice fed with regular water (Left) and 80 mM NaHCO<sub>3</sub> (pH 8.2) solution (Right) obtained on the IR scanner. The alkalization resulted in an ≈50% reduction of pHLIP accumulation in the kidney.



the distribution of pHLIP consisting of D-amino acids differs from the distribution of L-pHLIP, with more accumulation in tumors and/or less renal uptake, possibly as a result of better stability of the D-peptide in blood and/or less uptake by kidney. We also observed pHLIP accumulation in the skin, perhaps from the irritation caused by shaving the mice before imaging experiments to remove the background from hair fluorescence. We assume that skin uptake will be significantly less in nonshaved animals, which could lead to increased values in the CI. We did not observe strong accumulation of fluorescently labeled pHLIP in the liver.

A preliminary toxicity study was carried out on 4-week-old female and male mice. L-pHLIP and D-pHLIP were injected intravenously at the maximum concentration of 4 mg/kg, and animals were monitored for 2 months. No physiological or behavioral changes were detected.

## Discussion

Acidity characterizes the environment of cells that are partially starved for oxygen, such as highly proliferative cancer cells or macrophages at sites of inflammation and infection. Almost all solid tumors develop an acidic environment, known as the Warburg effect (Nobel Prize, 1931). The pHLIP bionanosyringe technology allows us to target and map acidity *in vivo*, which provides an opportunity for selective delivery of diagnostic or therapeutic agents to the sites of diseases. At physiological pH, the soluble form of pHLIP is favored, whereas at acidic pH the transmembrane  $\alpha$ -helix predominates. The pHLIP affinity for membranes at low pH (5.0) is 20 times higher than that at high pH (8.0) (Y.K.R., M.S., O.A.A., and D.M.E., unpublished data). We have shown that, at low pH, pHLIP can translocate cell-impermeable cargo molecules that are disulfide-linked to the C terminus across a cell membrane, where they are released in the cytoplasm by reduction of the disulfide bond (8, 9). Among the successfully translocated molecules are organic dyes, phalloidin (a polar, cyclic peptide), and 12-mer peptide nucleic acids. Neither the entry of pHLIP into the membrane nor the translocation of molecules into cells is mediated by endocytosis, binding to cell receptors, or formation of pores in cell membranes. Rather, entry and translocation result from the formation of a helix across the lipid bilayer because of the increase of peptide hydrophobicity associated with the protonation of an Asp residue at low pH. The replacement of two key Asp residues

located in the transmembrane part of pHLIP by Lys or Asn led to the loss of pH-sensitive membrane insertion into liposomes and RBCs *in vitro* and cancer cells *in vivo* and, consequently, to the loss of specific accumulation in tumors. We show that in a mouse breast adenocarcinoma model, fluorescently labeled pHLIP finds solid acidic tumors with high accuracy and accumulates at very early as well as advanced stages of tumor development. The fluorescence signal is stable for days and is approximately five times higher in tumors than in the healthy counterpart tissue. The pHLIP persistence stands in contrast to low-molecular-weight compounds, which typically wash out of the body in minutes. This property of pHLIP would allow hours of data collection from positron emission tomography (PET) or MRI agents to obtain excellent contrast ratios. Recently, we tested the distribution of a PET-imaging probe 1,4,7,10-tetraazacyclotetradecane-*N,N',N'',N'''*-tetraacetic acid (DOTA) covalently attached to the N terminus of pHLIP in male athymic mice bearing LNCaP tumors. DOTA-pHLIP afforded excellent tumor visualization in LNCaP tumor-bearing mice when using small-animal PET. Tumor/muscle ratios (standardized uptake value) were >6 at 24 h.<sup>1</sup> pHLIP also accumulates in comparable amounts in the kidney, which is not surprising because the kidney is a major site in the catabolism of low-molecular-weight proteins and has acidic regions. However, the uptake can be reduced significantly by providing mice with bicarbonate-buffered drinking water at pH 8.0 and perhaps by using the D-amino acid peptide. We did not observe a significant accumulation of pHLIP in the liver or other organs. pHLIP is not toxic for cells (8, 9), and preliminary studies suggest that it is not toxic for mice.

Recent developments have allowed the study of gene signatures of many cancer cells. The data indicate that a number of genes are up- and down-regulated in cancer, making it problematic to rely on any single tumor biomarker even for one type of cancer (24), whereas the physiological properties of the microenvironment of a majority (90%) of tumors, such as hypoxia, acidity, and changes in temperature, are considered promising environmental markers for tumor targeting (25, 26). Hypoxia and acidosis are hallmarks of tumors at both very early and advanced stages of tumor develop-

<sup>1</sup>Vavere, A. L., Andreev, O. A., Engelman, D. M., Reshetnyak, Y. K., Lewis, J. S. (2007) 17th International Symposium on Radiopharmaceutical Sciences (International Symposium on Radiopharmaceutical Sciences, Aachen, Germany), abstract.

ment. At hypoxic and acidic regions, chemotherapy and radiation therapies are significantly less effective (27). Moreover, recent data reveal the importance of inflammatory processes, which are associated with an elevated level of acidity, in tumor progression and even development (28, 29). Inflammatory mechanisms account for many features of various pathological processes such as rheumatoid arthritis or atherosclerotic plaque formation (30). Therefore, detection of an acidic environment might reveal possible sites of such diseases. pHLIP nanotechnology offers an approach for mapping areas of elevated acidity in the body, possibly enabling the study of pathological processes, diagnosis of diseases, treatment by delivery of molecules to affected areas, and monitoring of therapeutic outcomes.

## Methods

**Synthesis and Labeling of Peptides.** All peptides were prepared by solid-phase peptide synthesis using standard Fmoc (9-fluorenylmethylloxycarbonyl) chemistry and purified by reverse-phase chromatography (on a C18 column) at the W. M. Keck Foundation Biotechnology Resource Laboratory at Yale University. The peptide sequences used were:

- pHLIP: ACEQNPIYWARYADWLFTTPLL~~LL~~DLALLVDA-DEGTG
- K-pHLIP: ACEQNPIYWARYAKWLFTTPLL~~LL~~KLALLV-DADEGTG
- N-pHLIP: ACEQNPIWARYANWLFTTPLL~~LL~~NLALLV-DADEGTG.

We also synthesized a peptide with the same sequence as pHLIP from D-amino acids. The peptides were labeled with Cy5.5 (Amersham Bioscience) or Alexa750 (Invitrogen) according to supplier protocols. Free dyes were removed on Sephadex G-10 spin columns. The concentration and degree of labeling of peptides were determined by absorbance at 280 nm, 674 nm (Cy5.5), and 750 nm (Alexa750) with corrections for contributions of dyes at 280 nm according to supplied protocols. Molar extinction coefficients were used: peptide  $\epsilon_{280} = 13,940 \text{ M}^{-1}\cdot\text{cm}^{-1}$ ; Cy5.5  $\epsilon_{674} = 250,000 \text{ M}^{-1}\cdot\text{cm}^{-1}$ ; and Alexa750  $\epsilon_{750} = 240,000 \text{ M}^{-1}\cdot\text{cm}^{-1}$ . Peptide purity was checked by Tricine [N-tris(hydroxymethyl)methylglycine] SDS/PAGE followed by scanning gels on an IR scanner (Odyssey). The labeled peptides were stored at  $-80^\circ\text{C}$ .

**Liposome Preparation.** Large unilamellar vesicles were prepared by extrusion. 1-Palmitoyl-2-oleoyl-*sn*-glycero-3-phosphocholine (Avanti Polar Lipids, Inc.) in chloroform was evaporated on a rotary evaporator and dried under vacuum for several hours. The phospholipid film was rehydrated in 10 mM phosphate buffer (pH 8.0), vortexed for 2 h, and passed through 100-nm pores in the extruder 15 times. The concentration of the lipids was calculated by light scattering on a PC1 spectrofluorometer (ISS, Inc., Champaign, IL) with the set of excitation and emission monochromators at 700 nm and a vertical orientation of the excitation and emission polarizers. The scattering signal of the liposomes consisting of nonfluorescent lipids was compared with the signal of a known concentration of liposomes containing 1% phospholipids with fluorescently labeled head groups (phosphatidylethanolamine lissamine rhodamine B) prepared by exactly the same method described above.

**Purification of Human RBCs from Whole Blood.** Fresh whole human blood (tested negative for hepatitis B virus, hepatitis C virus, HIV1, HIV2, human T-lymphotrophic virus types 1 and 2, and syphilis) with sodium heparin was obtained from Bioreclamation (Hicksville, NY) and stored at  $4^\circ\text{C}$ . RBCs were purified within 48 h of withdrawal from human donors. Human RBCs were initially isolated by centrifugation at  $600 \times g$  for 20 min at  $4^\circ\text{C}$ . After removing the plasma and buffy layers by suction, the red cell pellet was resuspended in cold isotonic buffer containing 145 mM NaCl, 5

mM KCl, and 5 mM Hepes (pH 7.4) by trituration and then re-centrifuged at  $2000 \times g$  for 10 min at  $4^\circ\text{C}$ . The RBCs were washed with the isotonic buffer a total of four times to completely remove the plasma and buffy layers. The washed RBCs were resuspended in cold isotonic buffer (pH 7.4) to an approximate hematocrit level of 50% and stored at  $4^\circ\text{C}$ . All RBC samples were used for analysis within 24 h of purification and storage at  $4^\circ\text{C}$ .

**Human RBC Lysis Assay.** Cell lysis by pHLIP was measured spectrophotometrically by the amount of released hemoglobin from human RBCs. Samples of human RBCs were prepared at 1%, 5%, and 10% hematocrits in isotonic buffer containing 145 mM NaCl, 5 mM KCl, and 5 mM Hepes at pH 6.0 and pH 7.4. pHLIP, purified separately in isotonic buffer at pH 6.0 and pH 7.4, was added to the human RBC suspensions at 1%, 5%, and 10% hematocrits at final concentrations of 1, 5, and  $10 \mu\text{M}$ . All RBC samples were incubated at the various pHLIP concentrations for 1 h at room temperature. The samples were centrifuged at  $2,000 \times g$  for 10 min at  $t = 1$  min, 10 min, 30 min, and 1 h, and aliquots of the supernatant were collected. Absorption of the supernatant was recorded at 414 nm. Measurement of the absorption at 414 nm in comparison to 540 nm results in a 10-fold increase in the sensitivity of the assay (31). Human RBCs incubated in isotonic buffers at pH 6.0 and pH 7.4 at room temperature served as negative controls. As a positive control of 100% lysis, human RBCs were lysed with 10% Triton X-100 for 1 h at room temperature. Percent hemolysis at 1%, 5%, and 10% hematocrits and pHLIP concentrations of 1, 5, and  $10 \mu\text{M}$  was calculated as

$$100 - 100 \frac{A_{100\%} - A}{A_{100\%} - A_{0\%}}, \quad [1]$$

where  $A$  is the absorption measured at 414 nm.

**Tumor Mouse Model.** Female C3D2F1 mice ranging in age from 4 to 6 weeks and weighing from 14 to 16 g were obtained from Charles River Laboratories. The mice weighed  $\approx 20$  g at the time of peptide injection. Murine breast adenocarcinoma (CRL-2116) cell lines from the American Type Culture Collection were cultured in DMEM supplemented with 10% FBS, 100 units/ml penicillin, 0.1 mg/ml streptomycin, and 2 mM glutamine in a humidified atmosphere of 5%  $\text{CO}_2$  and 95% air at  $37^\circ\text{C}$ . Cancer cells were grown to 70% confluence and then harvested and resuspended in L-15 medium. Mouse tumors were established by s.c. injection of breast cancer cells ( $10^5$  to  $10^7$  cells per flank per 0.1 ml) in the right flank of adult female C3D2F1 mice.

**Arthritis Rat Model.** Male Lewis rats that ranged in age from 7 to 8 weeks and weighed from 180 to 200 g were obtained from Harlan Labs (Indianapolis, IN). The rats weighed  $\approx 300$  g at the time of peptide injection. Arthritis was induced in the right femorotibial joint of rats as described previously (12, 13). Briefly, on two occasions 2 weeks apart, the joint was injected s.c. with an emulsion (1.0 ml) of an equal mixture of BSA (methylated BSA) (0.5 mg; Sigma-Aldrich) and Freund's complete adjuvant (0.25 mg of *Mycobacterium tuberculosis*; Sigma-Aldrich). Six days after the second injection, 50  $\mu\text{g}$  of methylated BSA was injected into the right joint. The left knee joints of the rats received a sham injection of saline and were used as controls. The progression of inflammation was monitored by measuring the diameters of the right and left knee joints by using a micrometer. Beginning 1 week and lasting for the duration of 1 month after the induction of arthritis, the mean diameter of the right joints was significantly ( $P < 0.001$ ) higher than that of the left joints, highlighting the inflammatory process in the right leg. Student's unpaired 2-sample  $t$  test was used to test for differences in measurements between the right and left knee joints.  $P$  values of  $< 0.02$  were considered significant. After whole-body

imaging, the animals were killed, skin and muscle were removed from their legs, and fluorescence imaging was performed.

**Fluorescence and CD Measurements.** Trp fluorescence and CD measurements were carried out on a PC1 ISS spectrofluorometer and a Jasco (Easton, MD) 810 spectropolarimeter at 25°C, respectively, in phosphate buffer with adjusted pH. The concentrations of peptides and lipids used in this study were 5 and 600  $\mu\text{M}$ , respectively. The excitation wavelength was 295 nm to limit the excitation to only Trp fluorophores in the peptides. The fluorescence spectra were recorded from 310 to 400 nm with the spectral widths of excitation and emission slits set at 4 and 2 nm, respectively. The polarizers in the excitation and emission paths were set at the “magic” angle (54.7° from the vertical orientation) and vertically (0°), respectively, to reduce Wood’s anomalies from the reflecting holographic grating. The emission spectrum of an aqueous solution of L-Trp was used as a standard for the correction of protein spectra for the instrument spectral sensitivity. The intensities of the corrected spectra are proportional to the number of photons emitted per unit of time of indicated wavelength interval.

**Light Microscopy of RBCs.** Washed RBCs were prepared from whole human blood within 48 h of withdrawal from human donors (described above). A series of 1%, 5%, and 10% suspensions of washed human RBCs were made at pH 7.4 and 6.0 in isotonic buffers containing 145 mM NaCl, 5 mM KCl, and 5 mM Hepes. The RBC suspensions were then incubated in Eppendorf tubes for 15 min with 5  $\mu\text{M}$  pHLIP, K-PHLIP, and N-PHLIP at pH 7.4 and 6.0. Control RBC samples at pH 7.4 and 6.0 were then monitored for shape changes via light microscopy in addition to the RBC/peptide samples at pH 7.4 and 6.0. Samples were placed in Grace Bio-Labs CoverWell imaging chambers on glass slides that were treated with 2% dimethyldichlorosilane in 1,1,1-trichloromethane for 10 min and rinsed with methanol, ethanol, and water and allowed to dry before use in experiments to prevent the glass effect from inducing artificial echinocytosis. All samples were monitored via phase-contrast microscopy by using an Olympus IX71 inverted-fluorescence microscope with an  $\times 100$  objective and via differential interference contrast microscopy by using a Leitz Diaplan light microscope with Nomarski optics and an  $\times 100$  objective (data not shown).

**NIR Fluorescence Imaging of Whole Body, Tissue, and Organs.** Mice were injected with fluorescent pHLIP and imaged 4–21 days after cancer-cell implantation to mimic various stages of tumor development from early to advanced. When possible, tumor size was measured with a caliper. In some cases, at earlier stages, tumors were not visible by eye but were detectable by fluorescence imaging and later became visible. The inflammation sites in rats were imaged 20–30 days after induction of arthritis. The various amounts (100–200  $\mu\text{l}$  of 5–50  $\mu\text{M}$ ) of different types of pHLIP labeled with

Cy5.5 or Alexa750 were given as a single i.v. or i.p. injection to animals. Before imaging of mice or rats, their hair was removed with Nair (Carter-Wallace, New York). As a control, the free dyes incubated for several days in L-15 medium were injected at the same concentrations into mice carrying tumors. Incubation in L-15 was necessary to decrease the chemical reactivity of maleimide or NHS-ester moieties of dyes by their covalent binding to Cys or Lys amino acids, respectively, which are present in the L-15 solution. To increase the pH in the renal system, some mice were exposed to drinking water containing 80 mM  $\text{NaHCO}_3$  (pH 8.2) for 7–14 days. The imaging was performed while the animal was under anesthesia with a mixture of ketamine (90 mg/kg) and xylazine (9 mg/kg). Three imaging systems were used as our studies progressed: a homemade system with a light source (150-W xenon lamp) and double fiber-optic gooseneck [Dolan-Jenner Industries (Boxborough, MA) illuminator], an NIR-CCD camera (Hitachi, Tokyo), and appropriate filters (Omega Optical, Brattleboro, VT); an IR scanner (Odyssey); and a Kodak imaging station. To evaluate the signal/noise ratio of fluorescence images we calculated CI values according to that described by Jiang *et al.* (22). For the determination of tumor contrast, fluorescence mean, maximum, and minimal values of intensity, the SD and area of tumor and corresponding healthy tissue area were calculated by using NIH Image software and the area-of-interest function. The CI was measured according to the formula  $\text{CI} = [(F_{\text{tumor}} - F_{\text{auto}})/(F_{\text{norm}} - F_{\text{auto}})]$ , where  $F_{\text{tumor}}$  and  $F_{\text{norm}}$  are the fluorescence mean intensities of tumor and normal contralateral region of the same area, respectively, and  $F_{\text{auto}}$  is the autofluorescence from the corresponding region measured before injection. To evaluate the uptake of fluorescent peptides by internal organs and tissues, mice were dissected at various times after the injection of peptides. Organs and tissues were collected and their fluorescence was measured by using the homemade imager (each sample was measured separately by using the same set of optical parameters) or the IR Odyssey scanner (all samples were scanned at the same time).

All animal studies were conducted in accordance with the principles and procedures outlined in the National Institutes of Health Guide for the Care and Use of Animals. Approvals from the Institutional Animal Care and Use Committee at the University of Rhode Island were obtained before initiation of the study.

We thank Dr. W. Barry Piekos, Dr. Aftab Ahmed, and Gail Golomb Mello for technical assistance, the W. M. Keck Foundation Biotechnology Resource Laboratory at Yale University for peptide synthesis and purification; the Molecular Cellular and Developmental Biology’s electron microscopy facility at Yale University for use of its microscopes; and the Rhode Island IDeA Network of Biomedical Research Excellence core facility at University of Rhode Island (Grant P20RR016457 from the National Center for Research Resources, a component of the National Institutes of Health) for use of its IR imager. This work was supported in part by Department of Defense Grant PCRP CDMRP PC050351 (to Y.K.R.) and National Institutes of Health Grants GM070895 and GM073857 (to D.M.E.).

- Stubbs M, McSheehy PMJ, Griffiths JR, Bashford CL (2000) *Mol Med Today* 6:15–19.
- Naghavi M, John R, Naguib S, Siadat MS, Grasu R, Kurian KC, van Winkle WB, Soller B, Litovsky S, Madjid M, *et al.* (2002) *Atherosclerosis* 164:27–35.
- Izumi H, Torigoe T, Ishiguchi H, Uramoto H, Yoshida Y, Tanabe M, Ise T, Murakami T, Yoshida T, Nomoto M, *et al.* (2003) *Cancer Treat Rev* 29:541–549.
- Huang Y, McNamara JO (2004) *Cell* 118:665–666.
- Kellum JA, Song M, Li J (2004) *Crit Care* 8:331–336.
- Xiong ZG, Zhu XM, Chu XP, Minami M, Hey J, Wei WL, MacDonald JF, Wemmie JA, Price MP, Welsh MJ, *et al.* (2004) *Cell* 118:687–698.
- Hunt JF, Rath P, Rothschild KI, Engelman DM (1997) *Biochemistry* 36:15177–15192.
- Reshetnyak YK, Andreev OA, Lehnert U, Engelman DM (2006) *Proc Natl Acad Sci USA* 103:6460–6465.
- Andreev OA, Sandugu S, Engelman DM, Reshetnyak YK (2006) *Technical Proceedings of the 2006 Nanotech Conference* (Nano Science and Technology Institute, Cambridge, MA), Vol 2, pp 57–60.
- Weissleder R (2006) *Science* 312:1168–1171.
- Koo V, Hamilton PW, Williamson K (2006) *Cell Oncol* 28:127–139.
- Ballou B, Ernst LA, Waggoner AS (2005) *Curr Med Chem* 12:795–805.
- Elsaid KA, Jay GD, Chichester CO (2007) *Arthritis Rheum* 56:108–116.
- Andersson SE, Lexmuller K, Ekstrom GM (1998) *J Rheumatol* 25:1772–1777.
- Andersson SE, Lexmuller K, Johansson A, Ekstrom GM (1999) *J Rheumatol* 26:2018–2024.
- Reshetnyak YK, Koshevnik Y, Burstein EA (2001) *Biophys J* 81:1735–1758.
- Ponder E (1948) *Hemolysis and Related Phenomena* (J. and A. Churchill, London).
- Bessis M (1973) *Living Blood Cells and Their Ultrastructure* (Springer, New York).
- Markin VS (1981) *Biophys J* 36:1–19.
- Sheetz MP, Singer SJ (1974) *Proc Natl Acad Sci USA* 71:4457–4461.
- Lim GHW, Wortis M, Mukhopadhyay R (2002) *Proc Natl Acad Sci USA* 99:16766–16769.
- Jiang T, Olson ES, Nguyen QT, Roy M, Jennings PA, Tsieng RY (2004) *Proc Natl Acad Sci USA* 101:17867–17872.
- Wesson DE (1996) *Am J Physiol* 271:F132–F142.
- Bild AH, Yao G, Chang JT, Wang Q, Potti A, Chasse D, Joshi MB, Harpole D, Lancaster JM, Berchuck A, *et al.* (2006) *Nature* 439:353–357.
- Cairns R, Papandreou I, Denko N (2006) *Mol Cancer Res* 4:61–70.
- Coffey DS, Getzenberg RH, DeWeese TL (2006) *J Am Med Assoc* 296:445–448.
- Cerecetto H, Gonzalez M, Lavaggi ML (2006) *Med Chem* 2:315–327.
- Coussens LM, Werb Z (2002) *Nature* 420:860–867.
- Langowski JL, Zhang X, Wu L, Mattson JD, Chen T, Smith K, Basham, McClanahan T, Kastelein RA, Oft M (2006) *Nature* 442:461–465.
- Khan T, Soller B, Naghavi M, Casscells W (2005) *Cardiology* 103:10–16.
- Eschbach E, Scharsack JP, John U, Medlin LK (2001) *J Appl Toxicol* 21:513–519.